Journal of Engineering Mathematics **50:** 415–426, 2004.

Nonlinear capillary free-surface flows

J.-M. VANDEN-BROECK
School of Mathematics, University of East Anglia, Norwich NR4 7TJ, UK

Received 2 August 2004; accepted in revised form 28 August 2004

Abstract. Capillary free-surface flows are considered. The fluid is taken to be inviscid and incompressible and the flow to be irrotational. Particular attention is devoted to two-dimensional flows for which the free surfaces intersect rigid walls. These include cavitating flows and local flows at the front of a small object (probe or insect) moving at the surface of a fluid. A general study of the effect of surface tension on the possible singularities which can occur at the separation points is presented. The results confirm and generalise previous findings on the subject.

Key words: boundary-integral equations, cavitating flows, singularities on free-surfaces, surface tension

1. Introduction

Free-surface flows can be classified into two main classes. The first is the class of free-surface flows for which there are intersections between free surfaces and rigid surfaces. The prototype of this class is the flow due to a ship moving at the surface of a fluid (see for example [1, Section 3.10], [2,3]. The intersection is between the surface of the water and the hull of the ship. Others are jets falling from a nozzle, cavitating flows past an obstacle and flows under a sluice gate. The second class consists of free-surface flows with no interactions between rigid walls and free surfaces. Examples are bubbles rising in a fluid and free-surface flows generated by an object moving below a free surface (*e.g.*, a submarine). The prototype of this second class is a train of periodic travelling waves at the surface of a fluid. Here the train of waves extends periodically to infinity in the horizontal direction and the flow is studied independently of the way in which the waves are generated.

In this paper we concentrate mainly on pure capillary free-surface flows, *i.e.*, flows for which surface tension is taken into account but gravity is neglected. We also assume that the fluid is inviscid and incompressible and that the flow is irrotational. Crapper [4] found an exact solution for the prototype of the free-surface flows of the second class. More precisely, he obtained an analytic solution for nonlinear periodic waves travelling at a constant velocity at the surface of a fluid. His work was extended to finite depth by Kinnersley [5]. Kinnersley found that his solutions also describe waves propagating on a sheet and calculated both symmetric and antisymmetric solutions. Further branches of solutions were recently found by Blyth and Vanden-Broeck [6]. Other exact solutions for pure capillary free-surface flows were found by Crowdy [7]. In particular, waves in an annular geometry were calculated analytically. This work was generalised numerically by Blyth and Vanden-Broeck [8].

Solutions for pure capillary free-surface flows of the first class are described in this paper. We choose as our basic model the cavitating flow past a circular cylinder. We first describe free-streamline solutions (*i.e.*, solutions without surface tension) in Sections 2 and 3. Classical results on open cavities are reviewed in Section 2 and a boundary-integral-equation method

to compute cusped cavities is presented in Section 3. Cusped cavities were calculated analytically by Lighthill [9,10] for special geometries and numerically by Southwell and Vaisey [11]. We show that the cusped cavities form a continuation of the open cavities of Section 2. Our boundary-integral-equation method generalises the work of Lighthill [9,10] in the sense that it can be used for obstacles of arbitrary shapes.

The effect of surface tension T on the open cavities is considered in Section 4. In previous work [12–16], it was shown that the limit $T \to 0$ is singular in the sense that surface tension introduces discontinuities in slope at the separation points (*i.e.*, the points were rigid surfaces intersect free surfaces). Here we concentrate on solutions for which a prescribed contact angle is specified at the separation points. We show that the position of the separation points on the circular cylinder is uniquely defined by specifying the values of T. Although the results are presented for the specific problem of cavitating flows past a cylinder, similar results can be expected to hold whenever a free surface intersects a rigid smooth surface. Finally solutions in which waves appear in the far field are described in Section 5.

2. Free-streamline open cavities

In this section we review classical properties of free-streamline solutions, which will be useful in the remaining part of the paper. We consider the cavitating flow past a circle sketched in Figure 1. We denote by R the radius of the circle and by U the constant velocity of the flow at infinity. We assume that the fluid is inviscid and incompressible and that the flow is irrotational. We introduce Cartesian coordinates x and y and assume that the flow is symmetric with respect to the x-axis. The cavity is bounded by the streamlines BG and AD and by the portion BA of the circle. The cavity is open in the sense that it is unbounded as $x \to \infty$. We denote by p_∞ the constant pressure in the flow at infinity and by p_c the constant pressure in the cavity and we define the cavitation number C_c by the relation

$$C_c = \frac{p_\infty - p_c}{\frac{1}{2}\rho U^2}. \tag{2.1}$$

Bernoulli's equation implies that

$$\frac{1}{2}q^2 + \frac{p}{\rho} = \frac{1}{2}U^2 + \frac{p_\infty}{\rho} \tag{2.2}$$

everywhere in the fluid. Here q is the magnitude of the velocity and p is the pressure in the fluid. In the absence of surface tension, $p = p_c$ on the surface of the cavity. It follows from Equations (2.1) and (2.2) that

$$q^2 = U^2(1 + C_c) \tag{2.3}$$

on the surface of the cavity. Therefore the velocity q is constant on the free surfaces BC and AD. Such free surfaces are referred to as free streamlines.

Since the value of q on the free surface approaches U as $x \to \infty$, Equation (2.3) implies $C_c = 0$ and

$$q = U \quad \text{on} \quad BG \quad \text{and} \quad AD. \tag{2.4}$$

Solutions with $C_c \neq 0$ will be discussed in the next section.

We define dimensionless variables by using the radius R of the circle as the reference length and the velocity U as the reference velocity. We introduce the potential function $b\phi$,

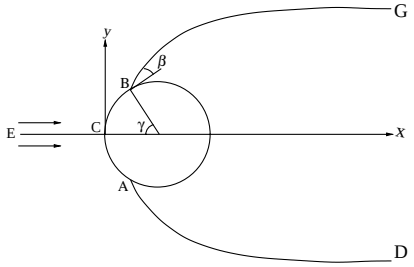

Figure 1. Sketch of the flow configuration and of the coordinates. When the surface tension T is zero, the free surfaces leave the cylinder tangentially and $\beta = 0$. When $T \neq 0$, the angle β can be different from zero.

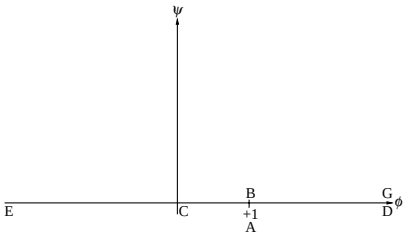

Figure 2. Sketch of the flow of Figure 1 in the complex potential plane.

the stream function $b\psi$ and the complex potential $f = \phi + \mathrm{i}\psi$. Without loss of generality we choose $\phi = 0$ at the point C and $\psi = 0$ on the streamlines $ECAD$ and $ECBG$. The constant b is defined so that $\phi = 1$ at the separation points A and B. The flow configuration in the complex potential plane is illustrated in Figure 2.

We introduce the complex velocity $u - \mathrm{i}v$ and define the function $\tau - \mathrm{i}\theta$ by the relation

$$u - \mathrm{i}v = \mathrm{e}^{\tau - \mathrm{i}\theta}. \tag{2.5}$$

Here u and v are the horizontal and vertical components of the velocity. The definition (2.5) has been used by many previous investigators. One of its advantage is that the curvature K of a streamline is given by the simple formula

$$K = \frac{\mathrm{e}^{\tau}}{b}\frac{\partial \theta}{\partial \phi} \tag{2.6}$$

We shall seek $\tau - \mathrm{i}\theta$ as an analytic function of $\phi + \mathrm{i}\psi$ in the half plane $\psi < 0$. The solution in $\psi > 0$ can then be obtained by symmetry. The boundary conditions on $\psi = 0$ are then given by

$$\theta = 0 \quad \text{on} \quad \psi = 0 \quad -\infty < \phi < 0, \tag{2.7}$$

$$\frac{\mathrm{e}^{\tau}}{b}\frac{\partial \theta}{\partial \phi} = 1 \quad \text{on} \quad \psi = 0 \quad 0 < \phi < 1, \tag{2.8}$$

$$\tau = 0 \quad \text{on} \quad \psi = 0 \quad 1 < \phi < \infty. \tag{2.9}$$

The condition (2.7) follows from symmetry. Equation (2.8) follows from Equation (2.6) and the fact that the curvature of the rigid boundary ACB is one. Relation (2.9) is the dynamic boundary condition (2.4) rewritten in terms of τ.

This completes the formulation of the problem. We seek $\tau - \mathrm{i}\theta$ as an analytic function of $\phi + \mathrm{i}\psi$ in $\psi < 0$ satisfying (2.7–2.9). We solve the problem by following the series-truncation method introduced by Brodetsky [17]. First we map the flow domain into the unit circle in the complex t-plane by the transformation

$$f^{1/2} = \left(t - \frac{1}{t}\right)\frac{1}{2\mathrm{i}}. \tag{2.10}$$

The flow configuration in the t-plane in shown in Figure 3. The rigid surface ACB is mapped on the circle $|t| = 1$ and the free surfaces AD and BG are mapped on the imaginary axis. The conditions (2.7–2.9) become

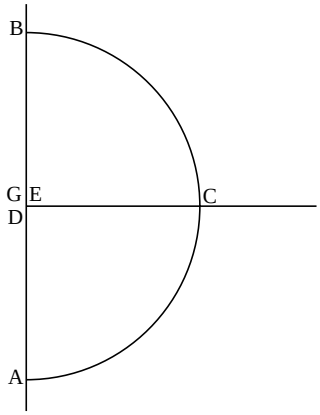

Figure 3. Sketch of the flow of Figure 1 in the complex t-plane.

$$\theta = 0 \quad \text{on} \quad 0 < t < 1, \tag{2.11}$$

$$\frac{e^{\tau}}{b}\frac{\partial \theta}{\partial \phi} = 1 \quad \text{on} \quad t = e^{i\sigma} \quad -\pi/2 < \sigma < 0, \tag{2.12}$$

$$\tau = 0 \quad -i < t < 0. \tag{2.13}$$

Here we have described the unit circle $|t| = 1$ by $t = e^{i\sigma}$.

Next we represent $\tau - i\theta$ by the expansion

$$\tau - i\theta = -\log\frac{1+t}{1-t} - \sum_{n=0}^{\infty} B_n t^n. \tag{2.14}$$

The idea behind Equation (2.14) is that a singularity in t occurs in the flow at the point C where the flow is locally a flow inside a right angle corner (see Figure 1). Therefore

$$u - iv \sim f^{1/2} \quad \text{as} \quad f \to 0 \tag{2.15}$$

Using Equations (2.5) and (2.10) yields $\tau - i\theta \sim \log(1-t)$ as $t \to 1$. Therefore

$$\tau - i\theta + \log\left(\frac{1+t}{1-t}\right) \tag{2.16}$$

is not singular and can be represented in the unit circle of the t-plane by a Taylor expansion. This leads to Equation (2.14). One might argue that other singularities occur at the separation points A and B. However, these singularities are automatically taken into account by Equation (2.10).

It can easily be checked that Equations (2.11) and (2.13) are satisfied by assuming that the coefficient B_n and real and that $B_n = 0$ when n is even. Therefore we rewrite Equation (2.14) as

$$\tau - i\theta = -\log\left(\frac{1+t}{1-t}\right) + \sum_{n=1}^{\infty} A_n t^{2n-1}. \tag{2.17}$$

We determine the coefficients A_n so that Equation (2.12) is satisfied. This is done numerically by series truncation and collocation. Thus we truncate the infinite series in Equation (2.17) after N terms and we satisfy Equation (2.12) at the mesh points

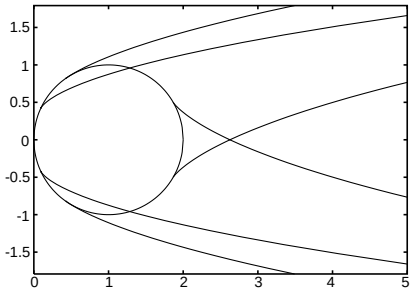

Figure 4. Computed free-surface profiles for $\gamma = 25^\circ$, $\gamma = \gamma^* \approx 55^\circ$ and $\gamma = 150^\circ$.

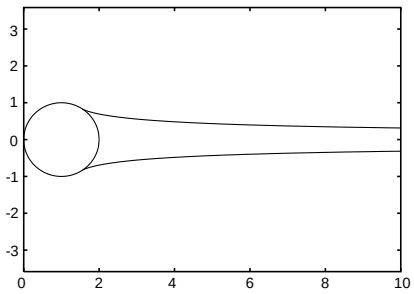

Figure 5. The cavitating flow corresponding to $\gamma = \gamma^{**} \approx 124^\circ$.

$$\phi_I = -\frac{\pi}{2N} I \quad I = 1, \ldots N. \tag{2.18}$$

This is achieved by using Equation (2.17) to evaluate the values of τ, θ and $\frac{\partial \theta}{\partial \phi}$ at the mesh points Equation (2.18) and by substituting these values in Equation (2.12). This leads to a system of N equations for the $N+1$ unknowns A_n, $n = 1, \ldots, N$ and b. The last equation is obtained by fixing the position of the separation points A and B by imposing

$$\theta(\phi_N) = \gamma - \pi/2, \tag{2.19}$$

where the angle γ is defined in Figure 1. The system is solved by Newton's method. The free-surface profiles are then obtained by integrating numerically the identity

$$\frac{1}{b}\left(\frac{\partial x}{\partial \phi} + \mathrm{i}\frac{\partial y}{\partial \phi}\right) = \mathrm{e}^{-\tau + \mathrm{i}\theta}. \tag{2.20}$$

The numerical results can be described in terms of the angle γ. Solutions can be obtained for all values $0 < \gamma < \pi$. However, only the solutions for $\gamma^* < \gamma < \gamma^{**}$, where $\gamma^* \approx 55^\circ$ and $\gamma^{**} \approx 124^\circ$, have a physical meaning for the cavitating flow past a circle.

For $\gamma < \gamma^*$, the solutions are not acceptable because the free surfaces enter the body (see Figure 4). They are, however, useful in describing the cavitating flow past the body obtained by cutting the circle along the straight line AB and retaining only the portion of the object on the left of AB.

For $\gamma > \gamma^{**}$, the solutions are not acceptable because the free surfaces cross each other (see Figure 4). The last acceptable solution for $\gamma = \gamma^{**}$ has free surfaces which approach asymptotically the x-axis as $x \to \infty$ (see Figure 5).

Physically acceptable solutions for $\gamma > \gamma^{**}$ can be obtained by considering cusped cavities. Cusped cavities were calculated numerically by finite differences by Southwell and Vaisey [11] and analytically for special geometries by Lighthill [9,10]. In the next section, cusped cavities are calculated numerically by a boundary-integral-equation method for obstacles of arbitrary shapes.

3. Free-streamline-closed cavities

Unwanted intersections of free surfaces occur in many applications. A classical example is the exact solution of Crapper [4] for nonlinear capillary waves travelling at a constant velocity

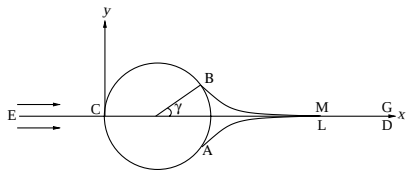

Figure 6. Sketch of the flow past a circular cylinder with a cusped cavity.

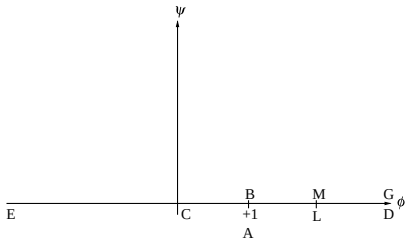

Figure 7. Sketch of the flow of Figure 6 in the complex potential plane.

at the surface of a fluid of infinite depth. Crapper's solutions form a one-parameter family of solutions. The parameter can be chosen as the steepness s of the waves (*i.e.*, the difference of heights between crests and troughs divided by the wavelength). For small values of s, the waves are close to linear sine waves. As s increases, the waves develop rounded crests and sharp troughs. When s reaches the critical value $s^* \approx 0{\cdot}73$, the free surface develops a point of contact with itself and a small trapped bubble at the trough of the wave. For $s > s^*$, the free surface is self-intersecting and the solutions lose their physical meaning. Vanden-Broeck and Keller [18] showed that physically acceptable solutions for $s > s^*$ can be obtained by preventing the free surface from self-intersecting. The resultant free-surface profiles for $s > s^*$ have trapped bubbles at the troughs like Crapper's solution for $s = s^*$. Since preventing self-intersection imposes an extra constraint on the solutions, an extra unknown is needed. This is achieved by finding the pressure in the trapped bubble as part of the solution.

We use an approach similar to that of Vanden-Broeck and Keller [18] to find physically acceptable cavitating flows for $\gamma > \gamma^{**}$. We prevent the crossing of the streamlines and seek a family of cusped cavities (see Figure 6). As we shall see, there is a cusped cavity for each value of $\gamma > \gamma^{**}$. These solutions approach the solution of Figure 5 as $\gamma \to \gamma^{**}$. In other words the x-coordinate of the cusps in Figure 6 tends to ∞ as $\gamma \to \gamma^{**}$ and the corresponding solutions approach that of Figure 5. As $\gamma \to 180^\circ$, the x-coordinate of the cusp tends to 2 and the cavity collapses to a point.

Following the work of Vanden-Broeck and Keller [18], we need to identify a new unknown to prevent the intersection of the streamlines. A natural choice is the pressure p_c in the cavity. This is motivated by the fact that cusped cavities are closed (they do not extend to infinity as the open cavities of Section 2) and we do not have to require $p_c = p_b$. Therefore our dynamic boundary condition on the free surfaces AL and BM of Figure 6 is

$$\tau = \frac{1}{2}\log(1 + C_c), \tag{3.1}$$

where the cavitation number C_c is found as part of the solution. As in Section 2, we define the potential function $b\phi$ and the stream function $b\psi$ and we choose b so that $\phi = 1$ at the separation points B and A. The flow configuration in the complex (ϕ, ψ) plane is illustrated in Figure 7.

We solve the problem by a boundary-integral-equation method. We derive the integral equation by applying a Cauchy-integral-equation formula in the (ϕ, ψ) plane to the function $\tau - i\theta$ with a contour consisting of the axis $\psi = 0$ and a semicircle, in $\psi < 0$, centered on $\phi = \psi = 0$, of arbitrary large radius. Since $\tau - i\theta \to 0$ as $\psi \to -\infty$, there is no contribution from the semicircle and we obtain after taking the real part

$$\tau(\phi)=\frac{1}{\pi}\int_{-\infty}^{\infty}\frac{\theta(\varphi)}{\varphi-\phi}\mathrm{d}\varphi. \tag{3.2}$$

The integral in Equation (3.2) is a Cauchy principal value and $\tau(\phi)$ and $\theta(\phi)$ denote the values of τ and θ on the streamline $\psi=0$. Since $\theta=0$ on EC and on LD, Equation (3.2) simplifies to

$$\tau(\phi)=\frac{1}{\pi}\int_{0}^{l}\frac{\theta(\varphi)}{\varphi-\phi}\mathrm{d}\varphi. \tag{3.3}$$

Here l is the value of ϕ at the cusp L.

The kinematic boundary condition on CA and the dynamic boundary condition Equation (3.1) imply

$$\frac{\mathrm{e}^{\tau}}{b}\frac{\partial\theta}{\partial\phi}=1 \quad 0<\phi<1, \tag{3.4}$$

$$\tau=\frac{1}{2}\log(1+C_c) \quad 1<\phi<l. \tag{3.5}$$

Finally we impose $y=0$ at the cusp by writing

$$\int_{0}^{l}\mathrm{e}^{-\tau(\varphi)}\sin\theta(\varphi)\mathrm{d}\varphi=0. \tag{3.6}$$

This completes the formulation of the problem. We seek $\tau(\phi)$ and $\theta(\phi)$ so that Equations (3.3–3.6) are satisfied. We solve the problem numerically. First we define the mesh points

$$\phi_I=\frac{I-1}{N-1} \quad I=1,\ldots,M \tag{3.7}$$

and the corresponding unknowns

$$\theta_I=\theta(\phi_I) \quad I=1,\ldots,M, \tag{3.8}$$

where $l=\frac{M-1}{N-1}$. We also use the midpoints

$$\phi_I^m=\frac{(\phi_I+\phi_{I+1})}{2} \quad I=1,\ldots,M-1. \tag{3.9}$$

We calculate $\tau(\phi_I^m)$ in terms of the unknowns Equation (3.8) by applying the trapezoidal rule to the integral in Equation (3.3) with a summation over the points Equation (3.7). The symmetry of the quadrature and of the distributions of mesh points enable us to calculate the Cauchy principal value as if it were an ordinary integral. Next we satisfy Equation (3.4) at the mesh points ϕ_I^m, $I=2,\ldots,N-1$ and Equation (3.5) at the mesh points ϕ_I^m, $I=N,\ldots,M-2$. The last three equations are given by Equation (3.6) and by the geometric conditions

$$\theta_1=-\frac{\pi}{2}, \quad \theta_M=0. \tag{3.10}$$

This system of algebraic equations is solved by Newton's method. Typical free-surface profiles are shown in Figure 8. As $\gamma\to\gamma^{**}$, $C_c\to 0$. As $\gamma\to 180^{\circ}$, $C_c\to-\infty$.

We note that the numerical procedure presented in this section is not restricted to a circular obstacle and that it can be generalised to obstacles of arbitrary shapes in the following way. First we denote by $F(x,y)=0$ the equation of the rigid boundary CA and calculate x and y on CA by the formulae

$$x(\phi)=\int_{0}^{\phi}\mathrm{e}^{-\tau(\varphi)}\cos\theta(\varphi)\mathrm{d}\varphi, \tag{3.11}$$

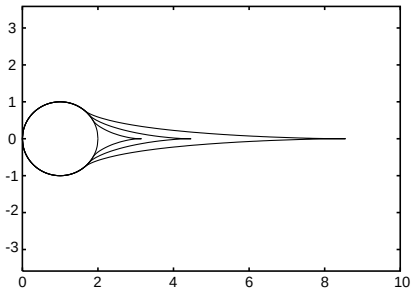

Figure 8. Three computed cusped cavities. The cavitation numbers C_c from the smallest cavity to the largest are $-0{\cdot}55$, $-0{\cdot}29$ and $-0{\cdot}1$, respectively.

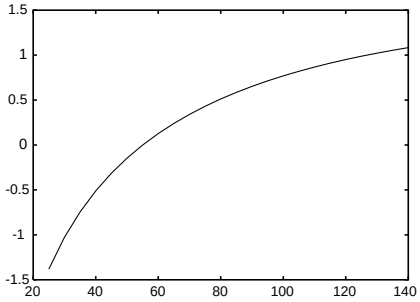

Figure 9. Values of the constant C in Equation (4.4) versus the angle γ.

$$y(\phi) = \int_0^{\phi} e^{-\tau(\varphi)} \sin\theta(\varphi) d\varphi. \tag{3.12}$$

We then apply the numerical procedure described above with the equations obtained by satisfying Equation (3.4) at the mesh points ϕ_I^m, $I = 2, \ldots, N-1$ by the new equations

$$F[x(\phi_I^m), y(\phi_I^m)] = 0 \quad I = 2, \ldots, N-1, \tag{3.13}$$

where $x(\phi)$ and $y(\phi)$ are defined by Equations (3.11) and (3.12).

Lighthill [9, 10] was able to obtain analytic solutions for cusped cavities by restricting his attention to obstacles of particular shape (for example a step in [10]). Our numerical results generalise Lighthill's results for obstacles of arbitrary shape.

The solutions derived in this section are examples of cavities with $C_c < 0$. Batchelor [19, pp. 503] notes that such cavities have not been observed, perhaps because the boundary layer at the rigid surface would separate before reaching the low-velocity region where the free streamlines begin.

Before concluding this section, let us mention that there are many cavity models with $C_c > 0$ (Riabouchinsky model, re-entrant jet model, Roskho model, etc). The reader interested in these models is referred to the books of Birkhoff and Zarantonello [20, Chapter 6] and Gurevich [21, Chapter 5].

4. Open cavities with surface tension

We consider the open-wake model of Section 2 with the effect of the surface tension T included in the dynamic boundary condition. The condition $p = p_c$ on the surface AD of the cavity is then replaced by

$$p = p_c - \frac{T}{\rho} K, \tag{4.1}$$

where K is the curvature of the free surface. Proceeding as in Section 2 we seek $\tau - i\theta$ as an analytic function of $\phi + i\psi$ in the lower half plane $\psi < 0$ of Figure 2, satisfying Equations (3.7) and (3.8) and

$$-\frac{e^{\tau}}{b}\frac{\partial \phi}{\partial \phi} = \frac{\alpha}{2}(e^{2\tau} - 1) \quad \text{on} \quad \psi = 0 \quad 1 < \phi < \infty. \tag{4.2}$$

Here α is Weber number defined by

$$\alpha = \frac{\rho U^2 R}{T}. \tag{4.3}$$

Free-streamline flows (without surface tension) are usually characterised by an infinite curvature of the free surface at the separation points (*i.e.*, the points where free surfaces intersect rigid surfaces). This does not affect solutions such as those presented in Sections 2 and 3 because the curvature of the free surface does not appear explicitly in the boundary conditions. However, it is no longer the case for flows with surface tension, because the curvature of the free surface appears explicitly in the dynamic boundary condition (see Equations (4.1) and (4.2)). Therefore we can expect free-surface flows with $T \neq 0$ to behave differently from flows with $T = 0$ and the limit as $T \to 0$ to be a singular limit. This is confirmed by the results presented below.

We start our investigation by calculating the curvature K_A of the free surface for the solution with $T = 0$ of Section 2 at the separation point A. Using Equations (2.6) and (2.17), we find

$$K_A = \frac{1}{b}\frac{\partial \theta}{\partial \phi} \approx -\frac{1}{2} C (b\phi - b)^{-1/2} \quad \text{as} \quad \phi \to 1, \tag{4.4}$$

where

$$C = -b^{-1/2} - b^{-1/2} \sum_{n=1}^{\infty} (-1)^{n+1} (2n-1) A_n. \tag{4.5}$$

A graph of C versus the angular position γ of the separation points is shown in Figure 9. The constant C vanishes when $\gamma = \gamma^* \approx 55^\circ$. Thus Equation (4.4) shows that the curvature of the free surface at the separation points is infinite unless $\gamma = \gamma^*$.

Ackerberg [22], Cumberbatch and Norbury [23], Vanden-Broeck [12–16] and others studied the flow configuration of Figure 1 (and related free-surface flows) in the limit as $T \to 0$. The results of Vanden-Broeck [12–16] showed that the inclusion of surface tension in the model of Section 2 does not remove the infinite curvature at the separation points. On the contrary, it makes the flow more singular by introducing a discontinuity in slope at the separation points. In other words, there is an angle β between the free surface and the tangent to the circle at the points A and B. The angle β is a function of γ and α. It is counted positive when the free surface lies above the tangent to the circle at the separation point B. Vanden-Broeck [13] showed that

$$\beta \approx \frac{C}{2} \left(\frac{\pi}{\alpha}\right)^{1/2} \quad \text{as} \quad \alpha \to \infty. \tag{4.6}$$

For $\gamma > \gamma^*$, Figure 9 shows that $C > 0$ and Equation (4.6) predicts $\beta > 0$. The flow near B is a flow inside an angle with a zero velocity at B. For $\gamma < \gamma^*$, Figure 9 shows that $C < 0$ and the values of β predicted by Equation (4.6) are then negative. The flow near B is then a flow around a corner with an infinite velocity at B. These results are only valid for α large. As $\alpha \to 0$, Equation (4.2) shows that the curvature of the free surfaces tends to zero. Since the flows are characterised by a constant velocity at infinity, the free surfaces must approach two horizontal straight lines. Therefore

$$\beta \to \gamma - \frac{\pi}{2} \quad \text{as} \quad \alpha \to 0. \tag{4.7}$$

Relation (4.7) shows that $\beta < 0$ in the limit $\alpha \to 0$ when $\gamma < \pi/2$. Relation (4.6) shows that $\beta > 0$ in the limit $\alpha \to \infty$ when $\gamma > \gamma^*$. If we assume that for a given value of γ, β is

a continuous function of α, there must exist for each value of α a particular value of $\gamma^* < \gamma < \pi/2$ for which $\beta = 0$ (*i.e.*, for which the flow leaves the circle tangentially). We describe these particular values of γ by the function

$$\gamma = g(\alpha). \tag{4.8}$$

This conjecture was confirmed by Vanden-Broeck [15] and [16]. Vanden-Broeck [15] computed the function $g(\alpha)$. Vanden-Broeck [16] showed that β is a continuous function of α by computing solutions with $\beta \neq 0$. These numerical results show that

$$g(\alpha) \to \gamma^* \quad \text{as} \quad \alpha \to \infty. \tag{4.9}$$

This implies that the limit $T \to 0$ can be used to select a particular solution with $T = 0$. In Section 2 we calculated solutions with $T = 0$. Then the dynamic boundary condition implies $\beta = 0$. We obtained solutions for all values of γ. When $T \neq 0$, solutions with $\beta = 0$ exist only for values of γ satisfying Equation (4.8). Taking the limit $\alpha \to \infty$, Equation (4.7) shows that we select the solution corresponding to $\gamma = \gamma^*$.

The solution corresponding to $\gamma = \gamma^*$ is known as the solution satisfying the Brioullin-Villat condition (see [20,21]). Therefore the selection mechanism based on the limit $T \to 0$ provides a new physical interpretation of the Brioullin-Villat condition.

So far we have mainly considered solutions with $\beta = 0$. It is of interest to look at solutions with $\beta \neq 0$. The angle β can then be interpreted as a contact angle whose value depends on the properties of the fluid and of the rigid boundary. Solutions with $\beta \neq 0$ can be computed by following the work of Vanden-Broeck [15]. We first map the flow of Figure 1 into the unit circle in the t plane by the transformation

$$t = \frac{1 + \mathrm{i} f^{1/2}}{1 - \mathrm{i} f^{1/2}}. \tag{4.10}$$

The flow configuration in the t-plane is shown in Figure 10. Next we note that the flow near A is locally a flow inside a corner with angle $\pi - \beta$ and that the flow near C is a flow inside a right angle corner. Therefore, using Equation (4.10) we obtain

$$u - \mathrm{i}v \sim (t - \mathrm{i})^{\beta/\pi} \quad \text{as} \quad t \to \mathrm{i}, \tag{4.11}$$

$$u - \mathrm{i}v \sim t - 1 \quad \text{as} \quad t \to 1. \tag{4.12}$$

Following the series truncation method of Section 2, we represent the complex velocity by

$$u - \mathrm{i}v = \mathrm{e}^{\tau - \mathrm{i}\theta} = (1 - t)(1 + t^2)^{\beta/\pi} \sum_{n=0}^{\infty} a_n t^n. \tag{4.13}$$

The multiplicative factors in front of the series in Equation (4.13) removes the singularity Equation (4.11). Therefore we can expect the series in Equation (4.13) to converge in the unit circle of the t-plane.

We describe points on the unit circle by $t = \mathrm{e}^{\mathrm{i}\sigma}$, $0 < \sigma < \pi$ and we rewrite Equations (4.2) and (2.8) as

$$-\frac{\mathrm{e}^{\tau}}{b} \frac{\cos^3(\sigma/2)}{\sin(\sigma/2)} \frac{\mathrm{d}\theta}{\mathrm{d}\sigma} = \frac{\alpha}{2}(\mathrm{e}^{2\tau} - 1) \quad \frac{\pi}{2} < \sigma < \pi, \tag{4.14}$$

$$\frac{\mathrm{e}^{\tau}}{b} \frac{\cos^3(\sigma/2)}{\sin(\sigma/2)} \frac{\mathrm{d}\theta}{\mathrm{d}\sigma} = 1 \quad 0 < \sigma < \frac{\pi}{2}. \tag{4.15}$$

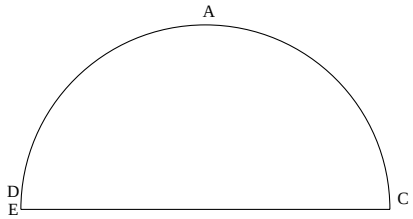

Figure 10. The flow of Figure 1 mapped into the t-plane by Equation (4.10).

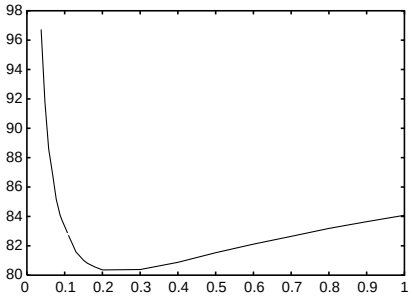

Figure 11. Values of γ versus α^{-1} for a given contact angle $\beta = 0{\cdot}04\pi$.

The coefficients a_n in Equation (4.13) are found so that Equations (4.14) and (4.15) are satisfied. This is achieved by series truncation and collocation as in Section 2. The reader is referred to [15] for details.

In Figure 11 we present values of γ versus α^{-1} for $\beta = 0{\cdot}04\pi$. This curve can be viewed as the equivalent of the curve Equation (4.8) but with $\beta = 0{\cdot}04\pi$ instead of $\beta = 0$. One interesting property in Figure 11 is that γ is not a monotonic function of α^{-1}. However, only one value of γ is selected for each value of the surface tension (*i.e.*, of α^{-1}). For α^{-1} small, γ increases rapidly. This behaviour can be described by substituting $\beta = 0{\cdot}04\pi$ in Equation (4.6) and noting that

$$C = 2(0{\cdot}04\pi)\left(\frac{\alpha}{\pi}\right)^{1/2}, \tag{4.16}$$

together with Figure 9, predicts that γ increases as α^{-1} decreases for α large.

5. Concluding remarks

We have presented numerical solutions for the flow configurations of Figures 1 and 6. The method used to compute the cusped cavities of Figure 6 generalises the work of Lighthill [9, 10] to obstacles of arbitrary shape. When the surface tension T is neglected, the free surfaces leave the cylinder tangentially and the angle β in Figure 1 is zero. When $T \neq 0$, the angle β is a function of the position γ of the separation point and of the Weber number α. We have studied families of solution in which the angle β is fixed (this corresponds to fixing the contact angle).

All the solutions with $T \neq 0$ presented in this paper are waveless in the far field (*i.e.*, as $x \to \infty$). This is consistent with the fact that the flow in Figure 1 is from left to right and that capillary waves would violate the radiation condition [1, Section 3.6]. However, capillary waves are acceptable if the flow is from right to left. Such configurations do not describe cavitating flows but can be used to model the flow at the front of a small object (insect or probe) moving at the surface of a fluid. Families of flows with capillary waves in the far field and $\beta \neq 0$ have recently been calculated (see [24]).

Acknowledgements

This work was support by EPSRC and the National Science Foundation. The author thanks Norman Riley for some very helpful comments and Scott Grandison for his help with the sketches.

References

1. M.J. Lighthill, *Waves in Fluids*. Cambridge: Cambridge University Press (1978) 504 pp.
2. W.T. Tsai and D.K. Yue, Computation of nonlinear free surface flows. *Ann. Rev. Fluid Mech.* 28 (1996) 249–278.
3. E. Parau and J.-M. Vanden-Broeck, Nonlinear two- and three-dimensional free surface flows due to moving disturbances. *Eur. J. Mech. B/Fluids* 21 (2002) 643–656.
4. G.D. Crapper, An exact solution for progressive capillary waves of arbitrary amplitude. *J. Fluid Mech.* 2 (1957) 532–540.
5. W. Kinnersley, Exact large amplitude waves on sheets of fluid. *J. Fluid Mech.* 77 (1976) 229–241.
6. M.G. Blyth and J.-M. Vanden-Broeck, New solutions for capillary waves on fluid sheets. *J. Fluid Mech.* 507 (2004) 255–264.
7. D.G. Crowdy, Exact solutions for steady capillary waves on a fluid annulus *J. Nonlinear Sci.* 9 (1999) 615–640.
8. M.G. Blyth and J.-M. Vanden-Broeck, New solutions for capillary waves on curved sheets of fluids. *IMA J. Appl. Math.* (submitted).
9. M.J. Lighthill, A note on cusped cavities. *Aero. Res. Coun. Rep. and Mem.* 2328 (1946).
10. M.J. Lighthill, On boundary layers and upstream influence, I. A comparison between subsonic and supersonic flows. *Proc. Roy. Soc. A* 217 (1953) 344–357.
11. R.V. Southwell and G. Vaisey, Fluid motions characterised by 'free' streamlines. *Phil. Trans. R. Soc. London A* 240 (1946) 117–161.
12. J.-M. Vanden-Broeck, The influence of capillarity on cavitating flow past a flat plate. *Quart. J. Mech. Appl. Math.* 34 (1981) 465–473.
13. J.-M. Vanden-Broeck, The influence of surface tension on cavitating flow past a curved obstacle. *J. Fluid Mech.* 133 (1983) 255–264.
14. J.-M. Vanden-Broeck, The effect of surface tension on the shape of the Kirchhoff jet. *Phys. Fluids* 27 (1984) 1933–1936.
15. J.-M. Vanden-Broeck, Numerical solutions for cavitating flow of a fluid with surface ten sion past a curved obstacle. *Phys. Fluids* 27 (1984) 2601–2603.
16. J.-M. Vanden-Broeck, Cavitating flow of a fluid with surface tension past a circular cylinder. *Phys. Fluids. A3* (1991) 263–266.
17. S. Brodetsky, Discontinuous fluid motion past circular and elliptic cylinders. *Proc. R. Soc. London A* 102 (1923) 1–14.
18. J.-M. Vanden-Broeck and J.B. Keller, A new family of capillary waves. *J. Fluid Mech.* 98 (1980) 161–169.
19. G.K. Batchelor, *Fluid Dynamics*. Cambridge: Cambridge University Press (1967) 615 pp.
20. G. Birkhoff and E.H. Zarantonello, *Jets, Wakes and Cavities*. New York: Academic Press (1957) 353 pp.
21. M. Gurevich, *Theory of Jets and Ideal Fluids*. New York: Academic Press (1965) 585 pp.
22. R.C. Ackerberg, The effects of capillarity on free-streamline separation. *J. Fluid Mech.* 70 (1975) 333–352.
23. E. Cumberbatch and J. Norbury, Capillarity modification of the singularity at a free-streamline separation point. *Q. J. Mech. Appl. Math.* 32 (1979) 303–312.
24. S. Tooley and J.-M. Vanden-Broeck, Waves and singularities in nonlinear capillary free-surface flows. *J. Engng. Math.* 43 (2002) 89–99.